Crystal structure of an enzyme displaying both inositol-polyphosphate-1-phosphatase and 3'-phosphoadenosine-5'-phosphate phosphatase activities: A novel target of lithium therapy

ARTICLE *in* JOURNAL OF MOLECULAR BIOLOGY · FEBRUARY 2002

Impact Factor: 4.33 · DOI: 10.1006/jmbi.2001.5271 · Source: PubMed

5 AUTHORS, INCLUDING:

Lynne Yenush
Universitat Politècnica de València
51 PUBLICATIONS **3,714** CITATIONS
SEE PROFILE

Pedro L Rodriguez
Universitat Politècnica de València
83 PUBLICATIONS **5,867** CITATIONS
SEE PROFILE

Tom L Blundell
University of Cambridge
654 PUBLICATIONS **38,834** CITATIONS
SEE PROFILE

doi:10.1006/jmbi.2001.5271 available online at http://www.idealibrary.com on IDEAL® J. Mol. Biol. (2002) 315, 677–685

JMB

Crystal Structure of an Enzyme Displaying both Inositol-polyphosphate-1-Phosphatase and 3′-Phosphoadenosine-5′-phosphate Phosphatase Activities: A Novel Target of Lithium Therapy

S. Patel[1]*, L. Yenush[2], P. L. Rodríguez[2], R. Serrano[2] and T. L. Blundell[1]

[1]*Department of Biochemistry University of Cambridge 80 Tennis Court Road Cambridge CB2 1GA, UK*

[2]*Instituto de Biología Molecular y Celular de Plantas Universidad Politécnica de Valencia-Consejo Superior de Investigaciones Científicas Camino de Vera s/n E-46022, Valencia, Spain*

**Corresponding author*

Lithium cations exert profound and selective psychopharmacological effects on ameliorate manic-depressive psychosis. Although lithium is an effective drug for both treatment and prophylaxis of bipolar disorder, the precise mechanism of action is not well understood. Lithium acts as both an uncompetitive and non-competitive inhibitor of several lithium-sensitive phosphatases with regard to substrate and magnesium cofactor, respectively. In this work, we report the crystal structure and reaction mechanism of *Rattus norvegicus* 3′-phosphoadenosine 5′-phosphate and inositol 1,4-bisphosphate phosphatase (RnPIP), a recently identified target of lithium therapy. This Li^+-sensitive enzyme plays a crucial role in several cellular processes, such as RNA processing, sulphation reactions and probably inositol recycling. RnPIP specifically removes the 3′-phosphate group of 3′-phosphoadenosine 5′-phosphate (PAP) and the 1′-phosphate group of inositol 1,4-bisphosphate ($I_{1,4}P_2$) producing AMP and inositol 4′-phosphate, respectively. The crystal structure of RnPIP complexed with AMP, Pi and magnesium ions at 1.69 Å resolution provides insight into the reaction mechanism of the hydrolysis of PAP. The core fold of the enzyme is equivalent to that found in other Li^+-sensitive phosphatases, such as inositol monophosphatase, but molecular modelling of $I_{1,4}P_2$ in the RnPIP active site reveals important structural determinants that accommodate this additional substrate. RnPIP is potently inhibited by lithium and, as the accumulation of PAP inhibits a variety of proteins, including sulphotransferases and RNA processing enzymes, this dual specificity enzyme represents a potential target of lithium action, in addition to inositol monophosphatases.

Keywords: inositol; 3′-phosphoadenosine 5′-phosphate; protein crystallography; sulphation; lithium

Introduction

Sulphation of key biomolecules is an absolute requirement in mammalian tissues, playing roles in deactivation and bioactivation of xenobiotics, inactivation of hormones and catecholamines, structure and function of macromolecules, and elimination of end-products of catabolism.[1–4] Sulphation of the chemokine receptor CCR5 enables HIV-1 entry into host cells, while proteoglycan sulphation controls interactions with growth factors.[5,6] The physiological importance of sulphation reactions is demonstrated by the pleiotropic phenotyes observed in brachymorphic mice, which are unable to synthesize the active high-energy form of sulphate, 3′-phosphoadenosine 5′-phosphosulphate (PAPS). This defect leads to abnormal hepatic detoxification, bleeding times and postnatal growth.[7]

The sulphotransferases are a family of enzymes that use PAPS as the activated sulphur source. Transfer is generally to hydroxyl groups, but also to unprotonated amine groups, and occurs in the

Abbreviations used: PAP, 3′-phosphoadenosine 5′-phosphate; PAPS, 3′-phosphoadenosine 5′-phosphosulphate; IMPase, inositol monophosphatase; IPPase, inositol polyphosphate 1-phosphatase; I_1, $_4P_2$, inositol 1,4 bisphosphate.

E-mail address of the corresponding author: joe@cryst.bioc.cam.ac.uk

0022-2836/02/040677–9 $35.00/0

Golgi lumen.[8] 3′-Phosphoadenosine 5′-phosphate (PAP) is the end-product of all sulphation reactions and acts as a competitive inhibitor of any enzyme that utilises PAPS.[9] PAPS is synthesised in the cytosol through a two-step reaction requiring two molecules of ATP and an inorganic sulphate ion. It is subsequently transported into the Golgi lumen *via* a PAPS translocase. The translocase displays an anti-port mechanism, in which PAP is returned to the cytosol for breakdown and is inhibited by PAP with a K_i of 6 μM.[10,11] M and P forms of the human phenolsulphotransferase have a K_i of 0.1 μM for PAP. PAP is also thought to act as a ribonucleotide monomer mimic for RNA processing enzymes, $5' \rightarrow 3'$ exoribonucleases, thereby preventing phosphodiester bond attack.[12] Recent reports have shown the accumulation of PAP in the brain of Li^+-treated bipolar patients.[13]

An enzymatic activity responsible for the breakdown of PAP to adenosine 5′-phosphate (AMP) and inorganic phosphate (Pi) was identified in mammals many years ago.[14] The molecular identification of this activity was described simultaneously by two groups, the first using a computer cloning strategy and the second, the functional complementation of yeast strains lacking the gene encoding Hal2p, a PAPase.[15,16] In both studies, *in vitro* experiments showed that in addition to the PAP phosphatase activity, the enzyme has inositol polyphosphate 1-phosphatase activity, although a discrepancy exists in the reported K_m values. Despite this difference, it seems clear that these mammalian enzymes represent an important connection between sulphate and inositol metabolism.

Inositol polyphosphate 1-phosphatase (IPPase) and inositol monophosphatase (IMPase) are thought to be therapeutic targets of lithium treatment for manic-depressive illnesses. Lithium acts as an uncompetitive and non-competitive inhibitor of these proteins, probably blocking inositol recycling and phosphoinositide metabolism.[17–19] RnPIP also displays sensitivity to lithium, and the inhibition of its human homologue may prove to have non-beneficial side-effects.[20]

Both IMPase and IPPase are representative members of a superfamily of Li^+-sensitive phosphatases that includes PAPases, such as Hal2p, and fructose bisphosphatases (FBPase). These enzymes are identified by two sequence motifs that contain key residues for magnesium ion coordination, and crystal structures have shown that they possess a common core fold of two domains, one $\alpha + \beta$ and one α/β.[21–24] Phylogenetic analysis suggests that these proteins originated from a common ancestor but sequence divergence has been extensive, as has the incorporation of extra secondary-structure elements.[15] FBPase and IMPase are universal enzymes. On the other hand, IPPases have been found only in mammals. In micro-organisms and plants, it is not clear how $I_{1,4}P_2$ hydrolysis occurs. However, to date, the PAPases are the only known phosphatases displaying this enzymatic activity, albeit with low affinity. By contrast, mammalian PIPases display high affinity for both PAP and $I_{1,4}P_2$, thus representing a class of enzymes that may be evolutionary intermediates between IPPases and PAPases.[15]

Here, we describe the crystal structure at 1.69 Å resolution of RnPIP complexed with magnesium ions, AMP and Pi. This is the first structure of an enzyme belonging to the family of novel dual specificity PAP and $I_{1,4}P_2$ phosphatases. We discuss the relationship of the structure of the rat enzyme to the human homologue, HsPIP, and identify a possible binding mode for $I_{1,4}P_2$. We investigate the similarity between RnPIP and Hal2p, a PAP phosphatase from yeast, and discuss the implications of this structure for the evolution of the superfamily.

Results

Crystal structure of RnPIP

The crystal structure of RnPIP was solved at 1.69 Å resolution by multiwavelength anomalous dispersion techniques using selenomethionated protein. The structure was built into electron density, phased by MAD to 2.35 Å resolution and extended to 1.69 Å by ARP/wARP for automatic backbone building.[25] After 15 rounds of free atom building, 99 % of the backbone was determined. The electron density at this stage was unambiguous and automatic side-chain addition was performed (Figure 1(c)). The first four N-terminal residues were disordered, most likely due to the presence of the fusion tag and a two-residue chain break was modelled between residues 78-81, which are part of a solvent-exposed loop structure. Side-chains lacking clear electron density were also excluded from the final model and consisted, primarily, of surface lysine residues. The quality of the model as denoted by PROCHECK[26] and WHATCHECK[27] was extremely high, providing evidence of the power of automated structure building (Table 1).

RnPIP has the characteristics of a superfamily of phosphatases, including Hal2p, that are all Li^+-sensitive. Although this superfamily is defined in SCOP[28] as sugar phosphatases, inositol is not strictly a sugar and we prefer to call them Li^+-sensitive phosphatases. They all contain an NH_2-terminal domain of the $\alpha + \beta$ class and a COOH-terminal domain of α/β with a mixed β-sheet. The mainly anti-parallel β-sheet of the N-terminal domain is comprised of β-strands from β3 to β8 with an α sub-domain containing α1 and α2. The C-terminal domain contains a mostly parallel β-sheet, comprising β-strands β9 to β13, sandwiched between two layers of α-helices (Figure 1(a) and (b)). The active site lies at the domain interface and is shielded by a hairpin β-sheet comprising residues 37-48. The protein was crystallized in the presence of PAP, catalytic magnesium and inhibitory lithium metal ions in the hope of trapping the

Table 1. Data collection, structure solution and refinement statistics

Data Collection	Native	Se-Met		
		Peak	Inflection	Remote
Wavelength (Å)	1.244	0.97911	0.97923	0.91841
No. unique reflections	38,442	14,420	14,427	12,269
Resolution (Å)	25-1.69		40-2.35	
Space group	$P2_12_12_1$			
Unit cell dimensions				
a (Å)	48.44		48.55	
b (Å)	74.49		78.53	
c (Å)	92.83		92.55	
Completeness (%) (outer shell)	99.6 (99.6)	99.2 (95.9)	99.1 (94.9)	85 (85)
Multiplicity (outer shell)	5.3 (5.1)	4.9 (4.9)	4.9 (4.9)	3.0 (3.0)
R_{merge} (%)[a] (outer shell)	9.0 (36.9)	6.5 (14.9)	7.3 (16.0)	8.3 (21.6)
Mean $I/\sigma I$ (outer shell)	12.4 (4.0)	14.8 (6.6)	13.2 (6.3)	8.7 (4.5)
R_{cullis} (iso/ano)[b]		0/0.70	0.62/0.86	0.78/0.90
Phasing power (iso/ano)[c]		0/2.08	1.11/1.48	0.91/1.21
Refinement				
Resolution range (Å)	57.7-1.69			
R-factor[d] (ove./1.77-1.69 Å)	14.7/19.0			
Free *R*-factor (ove./1.77-1.69 Å)	18.0/28.0			
Average *B*-factor ($Å^2$)	13.88			
RMSD bonds (Å)	0.014			
RMSD angles (deg.)	1.67			
RMSD planarity (Å)	0.007			

[a] $R_{merge} = \Sigma_{hkl}\Sigma_i|I_{hkl} - I_{hkl}|/\Sigma_{hkl}I_{hkl}$.
[b] R_{cullis} as defined by SHARP.
[c] Phasing power as defined by SHARP.
[d] $R\text{-factor} = \Sigma_{hkl}||F_{obs}| - |F_{calc}||/\Sigma_{hkl}|F_{obs}|$.

protein in a dead-end complex, as was seen in the crystal structure of another member of this family, Hal2p.[29] However, structure refinement gave clear density for the products of the reaction, AMP and inorganic phosphate, and all three metal-binding sites were found to contain magnesium ions. This result might suggest that the manner in which the protein packs into the crystal lattice prevents product release. Substrate and magnesium ions were found to be essential for crystal formation. Metal-binding site S1 maintains a magnesium ion in octahedral coordination *via* Glu74 OE1, Asp117 OD1, Val119 O, a water molecule and two oxygen atoms from Pi (Figure 2). The metal ion at site S2 is coordinated by Asp117 OD2, Asp120 OD1, Asp247 OD1, a water molecule, an oxygen atom from Pi and the 3′-hydroxyl group of AMP. The Hal2p structure suggests that S2 is likely to be the lithium-binding site. While S1 and S2 are thought to be involved in catalysis, the role of S3 is less obvious, as was found in inositol monophosphatase; the magnesium has one of the highest *B*-factors in the structure and a coordination sphere containing seven atoms, only one of which is protein (Glu74 OE1, an oxygen atom from Pi and five water molecules) within a 2.6 Å radius. The AMP occupies two pockets in the C-terminal domain, the distance between itself and Pi was 3 Å and confirmed the presence of product rather than substrate in the active site. The adenine ring is situated between His198 and the main chain of Gly242, forming a hydrophobic stacking interaction. The 5′-phosphate group maintains an extensive hydrogen-bonding network with Thr195 OG, His198 ND1, Gly220 NH, Lys224 NZ and three water molecules (Figure 3). HsPIP differs from RnPIP by only 27 residues, distributed throughout the protein. Most amino acid substitutions are conservative and all catalytic interactions are conserved, suggesting that the human protein will have a structure very similar to that of RnPIP.

Discussion

Comparison of RnPIP, Hal2p and IPPase substrate specificity

RnPIP is a member of the Li^+-sensitive phosphatase superfamily.[15,16] The structural similarity between RnPIP and other members of this superfamily, including fructose bisphosphatase, inositol mono/polyphosphate1-phosphatases and Hal2p is high, mainly due to the similar organisation of core secondary structure elements for metal ion coordination. However, sequence similarity between members is generally 25 % or less. The superfamily's divergence can be seen in the overall size of its members with the smallest, IMPase, having only 273 residues, while plant FBPase has over 500 residues, accounted for mainly by longer structural elements and loop regions (Figure 1(b) and Table 2).

Residues involved in metal ion coordination are absolutely conserved, although they play no direct role in substrate recognition. Analyses of the active sites of RnPIP, Hal2p and IPPase show clearly that RnPIP and Hal2p can accommodate both PAP and $I_{1,4}P_2$. Modelling of $I_{1,4}P_2$ into the RnPIP active site, based on the position of AMP, produced satisfactory hydrogen bonding networks and metal ion

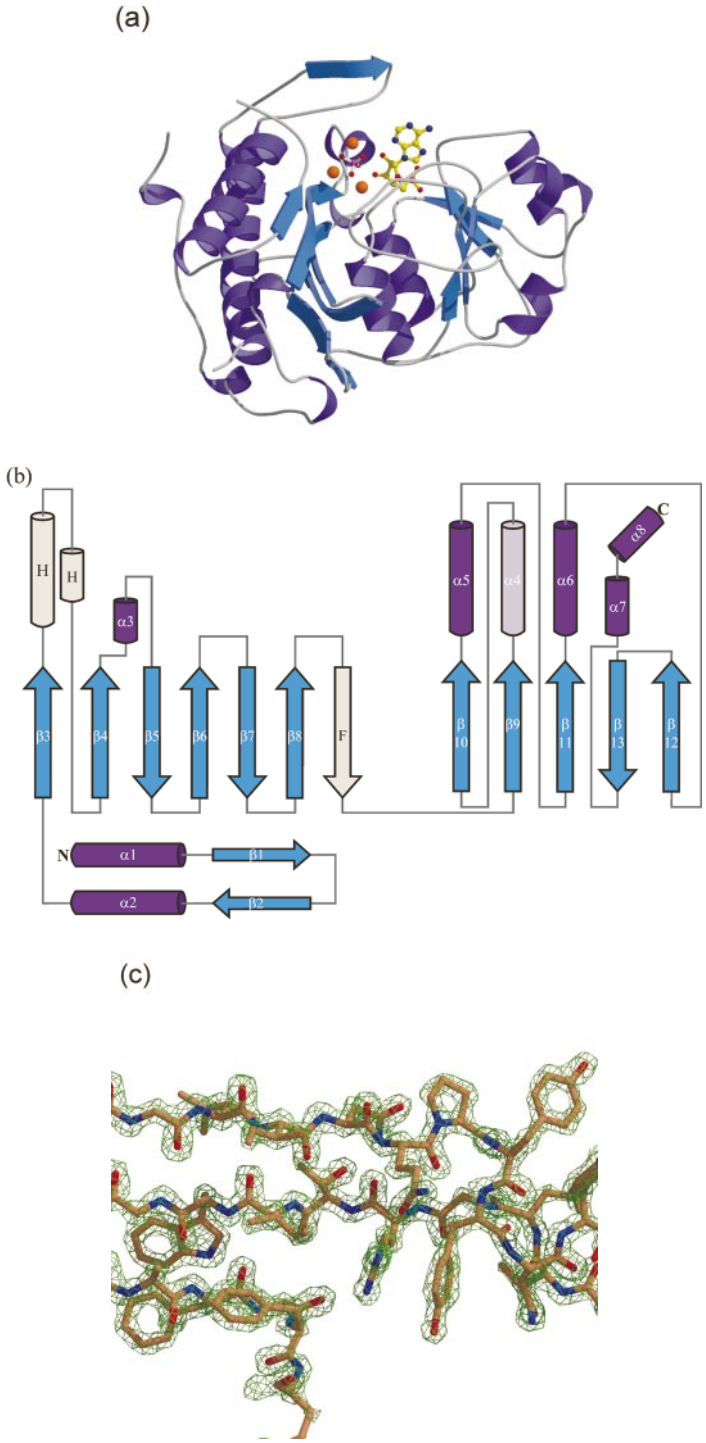

Figure 1. The structure of RnPIP. (a) A ribbon diagram showing the overall fold of RnPIP. The break in the chain represents the stretch of two amino acid residues that could not be seen clearly in the electron density maps (AMP is highlighted as a yellow stick model, the phosphate group is magenta). Three magnesium ions are shown as orange spheres. (b) A topology diagram showing conserved secondary structure in the Li^+-sensitive phosphatase superfamily. β-strands in light blue and α-helices in purple represent regions common to all members of the superfamily. Regions highlighted in grey are unique to specific classes of phosphates (H-Hal2p, F-FBPase and Hal2p). The light purple helix (α4) is found in all sugar phosphatases except inositol polyphosphate 1-phosphatase. (c) An example of the quality of electron density allowing unambiguous building to the RnPIP structure, map was contoured at 1.5σ.

coordination (Figure 4). By contrast, IPPase is capable of reacting only with $I_{1,4}P_2$, because of the inadequacy of stabilizing interactions for the PAP adenine ring. Stabilization for that ring comes in the form of a hydrophobic stacking interaction between His198 and Gly242 for RnPIP and His241 and Tyr288 for Hal2p. In IPPase, Lys270 and Thr312 replace these residues, with the latter in a

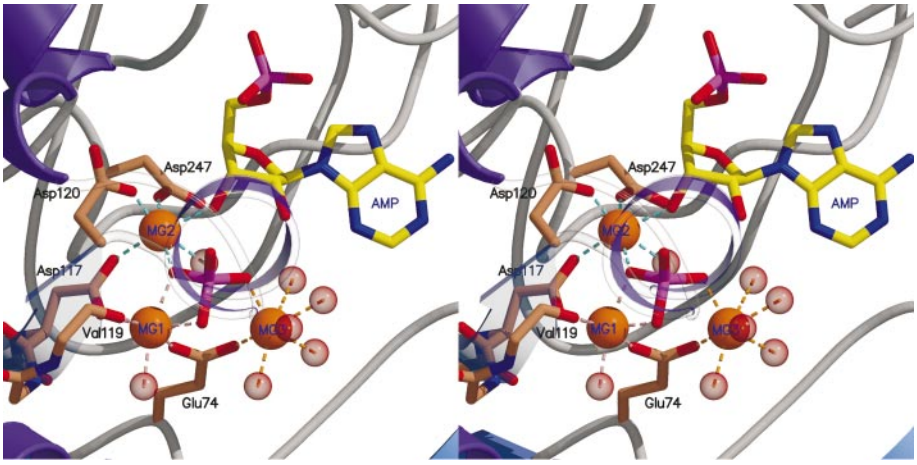

Figure 2. Wide-eye stereo view of the magnesium-binding sites. Key coordinating side-chains have been rendered as sticks and water molecules are highlighted as transparent red spheres. The AMP (yellow stick) and Pi (magenta stick) are also shown. Note that MG3 has seven ligands within its coordination sphere.

position to clash sterically with the nucleotide ring. The binding of the 5′-phosphate group of PAP in RnPIP and Hal2p is nearly identical and thus it is assumed that the equivalent 4′-phosphate group of $I_{1,4}P_2$ would bind in a similar manner to all three enzymes. The hydrogen bond network for RnPIP was described earlier and is comprised of Thr195 OG, His198 ND1, Gly220 NH, Lys224 NZ and three water molecules. For Hal2p, Lys267 NZ, Ser264 NH, His241 ND1 are equivalent, a water molecule replaces the threonine interaction for Hal2p and Arg281 NH1 and NH2 provide extra interactions with the O5′ and O4′ atoms. For IPPase, we predict that Lys294 NZ, Gly290 NH and Ser260 OB are involved in this network and that Lys270 NZ replaces the histidine interaction.

Table 2. Structural superposition of key members in the Li^+-sensitive phosphatase superfamily

	1FRP	1INP	2HHM	1QGX	RnPIP
1FRP	0.0 / 100	1.66 (127)	1.65 (163)	1.46 (147)	1.53 (123)
1INP	1.38/ 12.6	0.0 / 100	1.26 (145)	1.32 (164)	1.27 (193)
2HHM	1.40 / 12.2	1.22 / 17.2	0.0 / 100	1.32 (204)	1.23 (187)
1QGX	1.29 / 14.6	1.24 / 17.5	0.98 / 22.9	0.0 / 100	1.33 (182)
RnPIP	1.29 / 13.6	1.0 / 27.3	1.15 / 27.5	1.19 / 23.4	0.0 / 100

The coordinates used were fructose 1,4-bisphosphatase (PDB code 1FRP), human inositol monophosphatase (PDB code 2HHM), human inositol polyphosphate 1-phosphatase (PDB code 1INP), yeast PAP phosphatase (PDB code 1QGX) and RnPIP (PDB code 1JP4).

Cyan values are RMSD (Å) calculated on the basis of the position of 84 equivalent C^{α} positions in all the structures and percentage sequence identity with other superfamily members.

Yellow values are RMSD (Å) calculated on the basis of the pairwise structural alignments of superfamily members with the number of equivalent C^{α} positions given in parentheses.

Lithium sensitivity

RnPIP and its human homologue HsPIP have been shown to be sensitive to lithium (K_i of 0.6 and 0.3 mM, respectively) at levels that would block enzyme activity in patients undergoing lithium therapy for manic-depressive illness, typically 1 mM.[15,16,20] A molecular mechanism for lithium inhibition has been difficult to elucidate by X-ray crystallography because the ion has only two electrons, making it difficult to identify. However, enzyme kinetics for this family of enzymes has shown lithium to be an uncompetitive inhibitor with respect to both PAP and $I_{1,4}P_2$, interacting with the protein after substrate binding.[16] In Hal2p, lithium is likely to occupy the S2 binding site.[29] This site is equivalent to that seen in RnPIP and in the end-product state it maintains interactions with both the AMP molecule, through the newly formed 3′-hydroxyl group, and a phosphate oxygen atom. Lithium was known to prevent product release when complexed with IMPase[30] but, as yet, it is unclear whether it is capable of promoting hydrolysis or whether it simply displaces the S2 magnesium ion following phosphoester bond cleavage and traps the products in the active site. The S2 site is involved in the coordination of the phosphoester bond oxygen atom and the stabilization of the negative charge that would form during the transition state (Figure 5).

Mechanism

The dephosphorylation reaction of Li^+-sensitive phosphatases has an absolute requirement for magnesium ions and is most likely to proceed through the activation of a water molecule and subsequent nucleophilic attack on phosphorus.[31,32]

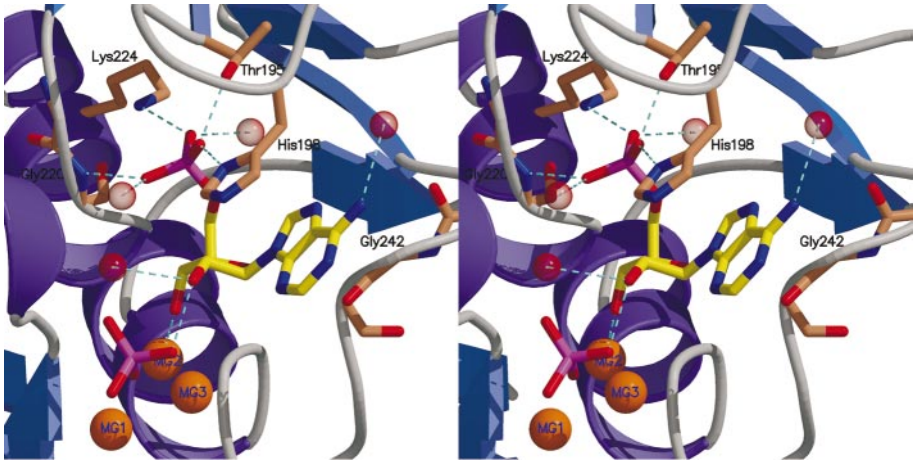

Figure 3. Wide-eye stereo view of the AMP-binding pocket. Key side-chains are rendered as sticks, the adenine ring is held in a hydrophobic stacking interaction with His198 and Gly242. The 5′-phosphate group makes a network of hydrogen bonds with side-chain and water molecules (red transparent spheres).

The number of magnesium ions required for this reaction to take place has been debated. The two-magnesium model proposes that S2 is responsible for coordinating the phosphoester bond and stabilizing the negative charge on the leaving group and the S1 site would coordinate the nucleophilic water molecule. Activation of this water molecule would come through hydrogen bonding with nearby glutamate and threonine residues, at positions 70 and 95 in IMPase.[22] However, the three-magnesium model, supported by our structure and that of a recently solved IMPase homologue, contradicts the above findings, in that the equivalent Glu74 interacts with both S1 and S3, metal ions, suggesting a role for the third site.[33] Thus, a water molecule coordinated by both S1 and S3, and activated by Thr122 would most likely be representative of the pre-reaction state. Thr122 is itself likely to be activated by a hydrogen bond with Asp51, increasing the nucleophilicity of the hydroxyl oxygen atom and allowing the formation of the hydroxyl nucleophile (Figure 5). A subsequent in-line attack of the phosphorus atom would lead to the formation of a trigonal bipyramidal transition state, with the charge stabilized by the S2 magnesium ion. The resulting product would display an inversion of absolute configuration about the phosphorus atom.

Thus, the resolution of the first dual specificity enzyme of this superfamily has defined important elements for substrate recognition, and for the reaction mechanism.

Material and Methods

Expression of RnPIP in *Escherichia coli*

The open reading frame (ORF) of RnPIP was amplified by PCR using the following primers: ORF5′, 5′-ATT AAT **GAA TTC** ATC *ATG* GCT TTC AGC CAC AAT-3′;

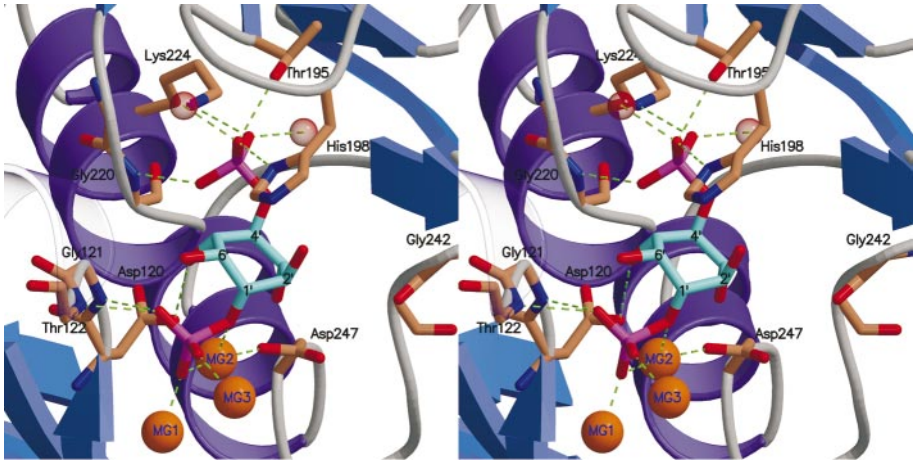

Figure 4. Wide-eye stereo view of inositol 1,4-bisphosphate docked into the RnPIP active site. The 4′-phosphate group of $I_{1/4}P_2$ (cyan sticks) maintains both protein and solvent interactions seen for the 5′-phosphate group of AMP. The 1′-phosphate group appears to be coordinated by all three magnesium ions (orange spheres). Asp120 is ideally placed to interact with the 5′-hydroxyl group.

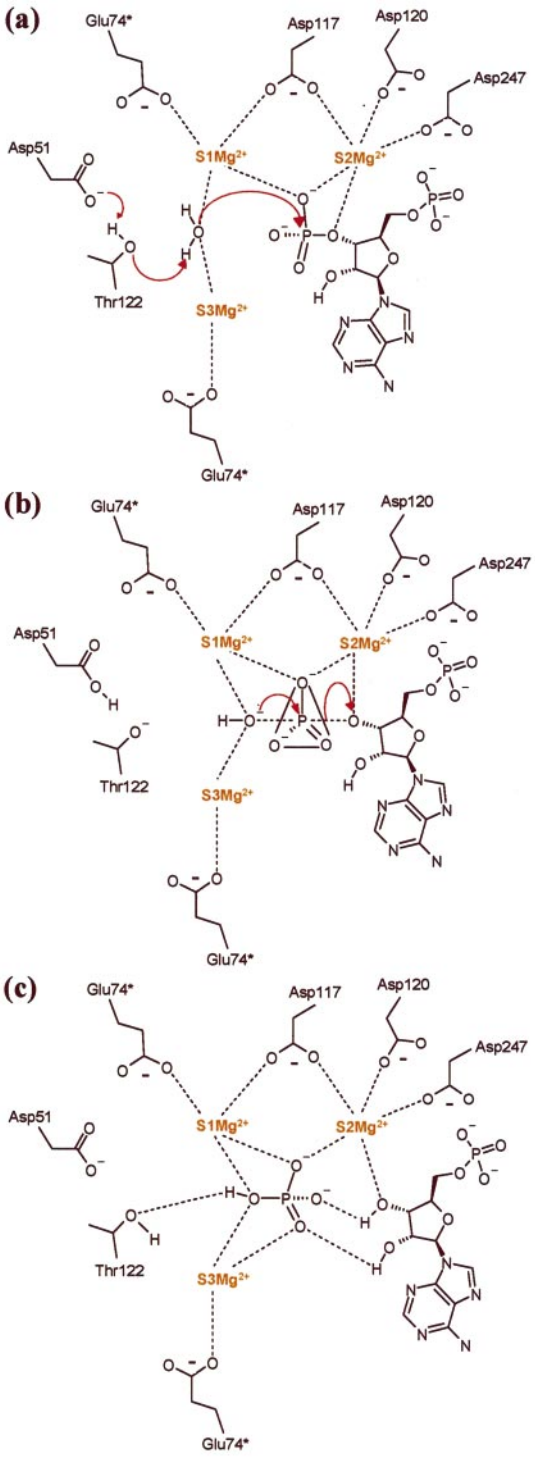

Figure 5. Mechanistic scheme for RnPIP activity. (a) Activation of the nucleophilic water molecule through a charge network between Asp51 and Thr122, and subsequent in-line attack of the phosphorus (magnesium and phosphate interactions are displayed as dotted lines and not all coordinations are shown for clarity). (b) Formation of a trigonal bipyramidal transition state, stabilized by the magnesium ions. (c) Product formation as transition state collapses with inversion of absolute configuration about phosphorus. *Glu74 coordinates magnesium ions in the S1 and S3 binding sites but for clarity has been drawn at two separate positions. This Figure was produced using ISIS Draw.

and ORF3′, 5′-ATT AAT **CTC GAG** *TCA* GGG AAT GAG TGC ACT-3′ (restriction sites are in bold face and start and stop codons are italicised). The resulting product was digested with *Eco*RI and *Xho*I, and ligated into the pET-28a histidine-tagged expression vector (Novagen). The RnPIP/pET28a vector was confirmed by sequencing, transformed into *E. coli* strain BL21 (DE3) and expressed in 2TY at 37 °C. SeMet expression was done in M9 medium supplemented with 4 % (w/v) glucose, 62 mg/l $MgSO_4$, 125 μg/l thiamine, 1 mg/l $FeSO_4$. Amino acids were added at 25 mg/l (Lys, Phe, Thr) and 12.5 mg/l (Ile, Leu, Val, SeMet). Cells were grown at 39 °C to inhibit methionine biosynthesis.

RnPIP purification

RnPIP was purified to homogeneity using a two-step protocol. The cells were resuspended in 20 mM Tris-HCl (pH 7.0), 500 mM NaCl, 5 mM β-mercaptoethanol and a Complete™ EDTA-free protease inhibitor tablet (Boehringer Mannheim). Cell lysis was achieved by use of a French press and the subsequent soluble extract was loaded onto a Talon Fast-Flow IMAC column (Clontech). The column was washed with wash buffer (20 mM Tris-HCl (pH 7.0), 500 mM NaCl, 5 mM β-mercaptoethanol, 15 mM imidazole). RnPIP was eluted using 250 mM imidazole and dialysed overnight into anion-exchange load buffer (20 mM Tris-HCl (pH 7.6), 10 mM NaCl, 5 mM β-mercaptoethanol). A linear gradient using 0-1 M NaCl was applied and RnPIP elutes between 90 and 140 mM NaCl. SeMet purification was similar to that of the native protein; however, all reducing agents were removed from buffers.

Crystallization, X-ray data collection, structure solution and refinement

Crystallization experiments were carried out in the presence of PAP and metal cofactors required for catalysis and inhibition. The protein was concentrated to 10 mg/ml, as determined by UV spectroscopy and a theoretical extinction coefficient,[34] and made to 5 mM $MgCl_2$, 6 mM Li_2SO_4 and 0.6 mM PAP. Experiments were carried out at room temperature and multiple hits were found from MDL crystal screens 1 and 2. Optimal single crystals were produced by vapour diffusion method using a protein to precipitant (20 % (w/v) PEG 8000, 0.2 M magnesium acetate, 0.1 M sodium cacodylate, pH 6.5) ratio of 1:1. Crystals appeared within a week and grew to full size within two weeks. The best cryoprotectant was found to be 20 % (w/v) glycerol and all data were collected at 100 K. Native X-ray data were collected to 1.69 Å resolution at station 9.6, Daresbury. Three-wavelength SeMet MAD data were collected to 2.35 Å at station BM14, ESRF-Grenoble. The arsenate from the cacodylate buffer in the cryoprotectant interfered with the successful collection of a Se X-ray fluorescence spectrum, hence wavelength selections for the peak and inflection were approximations. All data were integrated with DENZO and scaled using SCALEPACK.[35] The peak wavelength was used by SnB[36] to locate five of the six protein SeMet residues, four additional SeMet residues were in the fusion tag but were assumed to be disordered. The five sites were refined in SHARP[37] and the data solvent-flattened using DM[38] with histogram matching to 2.35 Å resolution. DM solvent-flattened phases together with high-resolution native data were used to run the ARP/wARP

warpNtrace automated backbone-building function.[25] A total of 15 building cycles, in conjunction with 200 REFMAC[39] restrained refinement cycles using all data, produced a model containing 297 out of the 301 backbone residues in the final model. The Sidetrace function was then used to add 218 side-chains. The remaining side-chains and ligands were built with manual intervention in O7[40] and refined using REFMAC. Side-chain errors were analysed using PROBE.[41] Water molecules were added using ARP/wARP and again refined with REFMAC. The quality of the model checked using PROCHECK and WHATCHECK.[26,27] Programs from the CCP4 package were also used.[42] All protein structure Figures were produced using MOLSCRIPT[43] and rendered using Raster3D.[44].

Superposition of Li^+-sensitive phosphatase and modelling of HsPIP and $I_{1,4}P_2$

Superposition of Li^+-sensitive phosphatase was performed using two methods. The first involved the superposition of all five protein structures using the COMPARER server (www-cryst.bioc.cam.ac.uk/~robert/cpgs/COMPARER/comparerstamp.html). The second method utilised the program TOP[45] with the protein structures aligned in pairs.

A sequence alignment between RnPIP and HsPIP involving no insertions or deletions was generated for residues 5-308. The modelling software, SCWRL,[46] was used to position 20 residue side-chains that differed between the sequences. The remaining structure was left unchanged. Two residues showed clashes and alternative rotamers were modelled into the HsPIP structure using O7.[40] $I_{1,4}P_2$ was built into the active sites of Hal2p and RnPIP by generating an $I_{1,4}P_2$ coordinate file from the structure of inositol hexaphosphate (PDB code 1thb). This $I_{1,4}P_2$ model was energy-minimised using SYBYL (Tripos, St. Louis) with TRIPOS Force Field[47] and a torsion library generated using the HIC-Up server.[48] Using the complexes of RnPIP or Hal2p with AMP bound into the active sites as a starting point, the 4′-phosphate group of $I_{1,4}P_2$ was overlaid with the 5′-phosphate group of AMP. Torsion adjustments were made in O7, and position of the $I_{1,4}P_2$ optimised in both active sites to improve hydrogen bonding interactions and reduce side-chain-ligand clashes.

Protein Data Bank accession codes

The coordinates and structure factor amplitudes are deposited in the RCSB Protein Data Bank with accession code 1JP4.

Acknowledgements

This work was supported by grant PB 98-0565-C04-01 of the Spanish Ministry of Education and Culture (Madrid). L.Y. was supported by a fellowship from the European Molecular Biology Organization. P.L.R. is supported by the Spanish Ministry of Science and Technology. We thank J.M. Lopez-Coronado for the RnPIP cDNA. S.P. and T.L.B. thank the Wellcome Trust and BBSRC for support. S.P. thanks D. Chirgadze, F. von Delft, M Hyvönen, E. Parisini and L. Pellegrini for their assistance. S.P. thanks G. Leonard for support during data collection at BM-14 ESRF.

References

1. Weinshilboum, R. M. (1986). Sulfate conjugation of neurotransmitters and drugs. Introduction. *Fed. Proc. Fed. Am. Soc. Expt. Biol.* **45**, 2220-2222.
2. Mulder, G. J. & Jakoby, W. B. (1990). Sulfation. In *Conjugation Reactions in Drug Metabolism* (Mulder, G. J., ed.), pp. 107-161, Taylor & Francis, London.
3. Falany, C. N. (1991). Molecular enzymology of human liver cytosolic sulfotransferases. *Trends Pharmacol. Sci.* **12**, 255-259.
4. Weinshilboum, R. & Aksoy, I. (1994). Sulfation pharmacogenetics in humans. *Chem. Biol. Interact.* **92**, 233-246.
5. Borgenstrom, M., Tienhaara, A., Spillmann, D., Salmivirta, M. & Jalkanen, M. (2001). Testosterone-induced growth of S115 mouse mammary tumor cells is dependent on heparan sulfate. *Expt. Cell Res.* **264**, 307-314.
6. Farzan, M., Mirzabekov, T., Kolchinsky, P., Wyatt, R., Cayabyab, M., Gerard, N. P. *et al.* (1999). Tyrosine sulfation of the amino terminus of CCR5 facilitates HIV-1 entry. *Cell,* **96**, 667-676.
7. Kurima, K., Warman, M. L., Krishnan, S., Domowicz, M., Krueger, R. C., Jr, Deyrup, A. & Schwartz, N. B. (1998). A member of a family of sulfate-activating enzymes causes murine brachymorphism. *Proc. Natl Acad. Sci. USA,* **95**, 8681-8685.
8. Klaassen, C. D. & Boles, J. W. (1997). Sulfation and sulfotransferases. 5. The importance of 3′-phosphoadenosine 5′-phosphosulfate (PAPS) in the regulation of sulfation. *FASEB J.* **11**, 404-418.
9. Rens-Domiano, S. S. & Roth, J. A. (1987). Inhibition of M and P phenol sulfotransferase by analogues of 3′-phosphoadenosine-5′-phosphosulfate. *J. Neurochem.* **48**, 1411-1415.
10. Ozeran, J. D., Westley, J. & Schwartz, N. B. (1996). Identification and partial purification of PAPS translocase. *Biochemistry,* **35**, 3695-3703.
11. Ozeran, J. D., Westley, J. & Schwartz, N. B. (1996). Kinetics of PAPS translocase: evidence for an antiport mechanism. *Biochemistry,* **35**, 3685-3694.
12. Dichtl, B., Stevens, A. & Tollervey, D. (1997). Lithium toxicity in yeast is due to the inhibition of RNA processing enzymes. *EMBO J.* **16**, 7184-7195.
13. Shaldubina, A., Agam, G. & Belmaker, R. H. (2001). The mechanism of lithium action: state of the art, ten years later. *Prog. Neuropsychopharmacol. Biol. Psychiatry,* **25**, 855-866.
14. Ramaswamy, S. G. & Jakoby, W. B. (1987). (2′)3′,5′-Bisphosphate nucleotidase. *J. Biol. Chem.* **262**, 10044-10047.
15. Lopez-Coronado, J. M., Belles, J. M., Lesage, F., Serrano, R. & Rodriguez, P. L. (1999). A novel mammalian lithium-sensitive enzyme with a dual enzymatic activity, 3′-phosphoadenosine 5′-phosphate phosphatase and inositol polyphosphate 1-phosphatase. *J. Biol. Chem.* **274**, 16034-16039.
16. Spiegelberg, B. D., Xiong, J. P., Smith, J. J., Gu, R. F. & York, J. D. (1999). Cloning and characterization of a mammalian lithium-sensitive bisphosphate 3′-nucleotidase inhibited by inositol 1,4-bisphosphate. *J. Biol. Chem.* **274**, 13619-13628.
17. Inhorn, R. C. & Majerus, P. W. (1988). Properties of inositol polyphosphate 1-phosphatase. *J. Biol. Chem.* **263**, 14559-14565.
18. Nahorski, S. R., Ragan, C. I. & Challiss, R. A. (1991). Lithium and the phosphoinositide cycle: an example

of uncompetitive inhibition and its pharmacological consequences. *Trends Pharmacol. Sci.* **12**, 297-303.
19. Strasser, F., Pelton, P. D. & Ganzhorn, A. J. (1995). Kinetic characterization of enzyme forms involved in metal ion activation and inhibition of myo-inositol monophosphatase. *Biochem. J.* **307**, 585-593.
20. Yenush, L., Belles, J. M., Lopez-Coronado, J. M., Gil-Mascarell, R., Serrano, R. & Rodriguez, P. L. (2000). A novel target of lithium therapy. *FEBS Letters,* **467**, 321-325.
21. York, J. D. & Majerus, P. W. (1990). Isolation and heterologous expression of a cDNA encoding bovine inositol polyphosphate 1-phosphatase. *Proc. Natl Acad. Sci. USA,* **87**, 9548-9552.
22. Bone, R., Springer, J. P. & Atack, J. R. (1992). Structure of inositol monophosphatase, the putative target of lithium therapy. *Proc. Natl Acad. Sci. USA,* **89**, 10031-10035.
23. Zhang, Y., Liang, J. Y. & Lipscomb, W. N. (1993). Structural similarities between fructose-1,6-bisphosphatase and inositol monophosphatase. *Biochem. Biophys. Res. Commun.* **190**, 1080-1083.
24. York, J. D., Ponder, J. W. & Majerus, P. W. (1995). Definition of a metal-dependent/Li(+)-inhibited phosphomonoesterase protein family based upon a conserved three-dimensional core structure. *Proc. Natl Acad. Sci. USA,* **92**, 5149-5153.
25. Perrakis, A., Sixma, T. K., Wilson, K. S. & Lamzin, V. S. (1997). wARP: improvement and extension of crystallographic phases by weighted averaging of multiple refined dummy atomic models. *Acta Crystallog. sect. D,* **53**, 448-455.
26. Laskowski, R. A., Macarthur, M. W., Moss, D. S. & Thornton, J. M. (1993). PROCHECK - a program to check the stereochemical quality of protein structures. *J. Appl. Crystallog.* **26**, 283-291.
27. Rodriguez, R., Chinea, G., Lopez, N., Pons, T. & Vriend, G. (1998). Homology modelling, model and software evaluation: three related resources. *CABIOS,* **14**, 523-528.
28. Murzin, A. G., Brenner, S. E., Hubbard, T. & Chothia, C. (1995). SCOP: a structural classification of proteins database for the investigation of sequences and structures. *J. Mol. Biol.* **247**, 536-540.
29. Albert, A., Yenush, L., Gil-Mascarell, M. R., Rodriguez, P. L., Patel, S., Martinez-Ripoll, M., Blundell, T. L. & Serrano, R. (2000). X-ray structure of yeast Hal2p, a major target of lithium and sodium toxicity, and identification of framework interactions determining cation sensitivity. *J. Mol. Biol.* **295**, 927-938.
30. Shute, J. K., Baker, R., Billington, D. C. & Gani, D. (1988). Mechanism of the *myo*-inositol phosphatase reaction. *J. Chem. Soc. Chem. Commun.* **00**, 626-628.
31. Leech, A. P., Baker, G. R., Shute, J. K., Cohen, M. A. & Gani, D. (1993). Chemical and kinetic mechanism of the inositol monophosphatase reaction and its inhibition by Li^+. *Eur. J. Biochem.* **212**, 693-704.
32. Pollack, S. J., Atack, J. R., Knowles, M. R., McAllister, G., Ragan, C. I., Baker, R. *et al*. (1994). Mechanism of inositol monophosphatase, the putative target of lithium therapy. *Proc. Natl Acad. Sci. USA,* **91**, 5766-5770.
33. Johnson, K. A., Chen, L., Yang, H., Roberts, M. F. & Stec, B. (2001). Crystal structure and catalytic mechanism of the MJ0109 gene product: a bifunctional enzyme with inositol monophosphatase and fructose 1,6-bisphosphatase activities. *Biochemistry,* **40**, 618-630.
34. Gill, S. C. & von Hippel, P. H. (1989). Calculation of protein extinction coefficients from amino acid sequence data. *Anal. Biochem.* **182**, 319-326.
35. Otwinowski, Z. & Minor, W. (1997). Processing of X-ray diffraction data collected in oscillation mode. *Methods Enzymol* **276**, 307-326.
36. Weeks, C. M. & Miller, R. (1999). Optimizing shake-and-bake for proteins. *Acta Crystallog. sect. D,* **55**, 492-500.
37. de la Fortelle, E. & Bricogne, G. (1997). Maximum-likelihood heavy atom parameter refinement of multiple isomorphous replacement and multiwavelength anomalous diffraction methods. *Methods Enzymol.* **276**, 472-494.
38. Cowtan, K. (1994). An automated procedure for phase improvement by density modification. *Joint CCP4 ESF-EACBM Newsletter Protein Crystallog.* **31**, 34-38.
39. Murshudov, G. N., Vagin, A. A. & Dodson, E. J. (1997). Refinement of macromolecular structures by the maximum-likelihood method. *Acta Crystallog. sect. D,* **53**, 240-255.
40. Jones, T. A., Zou, J. Y., Cowan, S. W. & Kjeldgaard, M. (1991). Improved methods for model building in electron density maps and the location of errors in these models. *Acta Crystallog. sect. A,* **47**, 110-119.
41. Word, J. M., Lovell, S. C., LaBean, T. H., Taylor, H. C., Zalis, M. E., Presley, B. K. *et al*. (1999). Visualizing and quantifying molecular goodness-of-fit: small-probe contact dots with explicit hydrogen atoms. *J. Mol. Biol.* **285**, 1711-1733.
42. Baily, S. (1994). The CCP4 suite - programs for protein crystallography. *Acta Crystallog. sect. D,* **50**, 760-763.
43. Kraulis, P. J. (1991). MOLSCRIPT - a program to produce both detailed and schematic plots of protein structures. *J. Appl. Crystallog.* **24**, 946-950.
44. Merritt, E. A. & Murphy, M. E. P. (1994). Raster3D version-2.0 - a program for photorealistic molecular graphics. *Acta Crystallog. sect. D,* **50**, 869-873.
45. Lu, G. (2000). A new method for protein structure comparisons and similarity searches. *J. Appl. Crystallog.* **33**, 176-183.
46. Bower, M. J., Cohen, F. E. & Dunbrack, R. L., Jr (1997). Prediction of protein side-chain rotamers from a backbone-dependent rotamer library: a new homology modeling tool. *J. Mol. Biol.* **267**, 1268-1282.
47. Clark, M., Cramer, R. D. I. & van Opdenbosch, N. (1989). Validation of the general purpose tripose 5. 2 force field. *J. Comp. Chem.* **10**, 982-1012.
48. Kleywegt, G. J. & Jones, T. A. (1998). Databases in protein crystallography. *Acta Crystallog. sect. D,* **54**, 1119-1131.

Edited by R. Huber

(Received 24 July 2001; received in revised form 7 November 2001; accepted 10 November 2001)